

Supergravity inflation on a brane

Mudassar Sabir,^{1,*} Waqas Ahmed,^{2,†} Yungui Gong,^{1,‡}

Shan Hu,^{3,§} Tianjun Li,^{4,5,¶} and Lina Wu^{6,**}

¹*School of Physics, Huazhong University of Science
and Technology, Wuhan, Hubei 430074, China*

²*School of Physics, Nankai University, Nankai District, Tianjin, China*

³*Department of Physics, Faculty of Physics and
Electronic Sciences, Hubei University, Wuhan, China*

⁴*CAS Key Laboratory of Theoretical Physics, Institute of Theoretical Physics,
Chinese Academy of Sciences, Beijing 100190, China*

⁵*School of Physical Sciences, University of Chinese Academy of Sciences, Beijing, China*

⁶*School of Science, Xi'an Technological University, Xi'an, China*

(Dated: December 20, 2024)

Abstract

We discuss supergravity inflation in braneworld cosmology for the class of potentials $V(\phi) = \alpha\phi^n \exp(-\beta^m \phi^m)$ with $m = 1, 2$. These minimal SUGRA models evade the η problem due to a broken shift symmetry and can easily accommodate the observational constraints. Models with smaller n are preferred while models with larger n are out of the 2σ region. Remarkably, the field excursions required for 60 e -foldings stay sub-planckian $\Delta\phi < 1$.

* msabir@hust.edu.cn

† waqasmit@nankai.edu.cn

‡ yggong@hust.edu.cn

§ hushan@hubu.edu.cn

¶ tli@itp.ac.cn

** wulina@xatu.edu.cn

I. INTRODUCTION

It is well known that our universe may have experienced accelerated expansion, *i.e.*, cosmic inflation [1–4], at a very early stage of its evolution as evident from the temperature fluctuations and observations of polarization spectrum of the cosmic microwave background radiation. It provides a convincing explanation for the observed large scale homogeneity and isotropy of the universe. Inflation may have taken place at the GUT unification scale or below [5–9] and is assumed to be described by the effective field theories (EFTs) [10]. Such EFTs can only be trusted if they can be successfully embedded in a theory of quantum gravity. Models in standard general relativity suffer from the problem of super-planckian field excursions.

The field excursion is related to the tensor-to-scalar ratio r by the Lyth bound [11, 12] as

$$\Delta\phi \simeq N\sqrt{\frac{r}{8}}, \quad (1)$$

where N is the number of e -folds before the end of inflation. To avoid super-planckian field excursions and flatness requirement of $N \geq 50$, we find $r \sim 0.003$. This value lies on the edge of observability for the future LiteBIRD, an experiment designed for the detection of B-mode polarization pattern embedded in the Cosmic Microwave Background anisotropies [13].

Supersymmetry provides the most promising extension for the Standard Model of particle physics. However, it is still regarded as a global symmetry. In the context of AdS/CFT [14, 15], it was argued in Ref. [16] that no global symmetries can exist in a theory of quantum gravity. It is thus believed that supersymmetry must be a gauged symmetry, *i.e.* supergravity. The theory of supergravity is a natural framework for inflation model building [17, 18]. In this note, we consider a class of inflationary models with the potential $V(\phi) = \alpha\phi^n \exp(-\beta^m \phi^m)$ that can be embedded in supergravity with a small shift symmetry breaking term in Kähler potential [19]. We show that some of the models not only meet the swampland criteria but also satisfy all the current experimental constraints from TT, TE, EE+lowE+lensing+BK14+BAO data in Ref. [20].

II. BRANE INFLATION IN SUPERGRAVITY WITH BROKEN SHIFT SYMMETRY

In Ref. [19], a class of inflationary models were derived from supergravity with the potential of the following form,

$$V(\phi) = \alpha \phi^n \exp(-\beta^m \phi^m), \quad m = 1, 2; \quad n = 1, 3/2, 2. \quad (2)$$

It was shown that such kind of inflaton potentials can be realized with a small shift symmetry breaking term in Kähler potential. We now examine the embedding of such models in the brane context.

In braneworld cosmology, our 4-dimensional world is a 3-brane embedded in a higher-dimensional bulk. The Friedmann equation then gets a ρ^2 correction as [21–25]

$$H^2 = \frac{1}{3M_p} \rho \left(1 + \frac{\rho}{2\lambda} \right), \quad (3)$$

where λ is the brane tension parameter relating 4-dimensional Planck scale M_4 and 5-dimensional Planck scale M_5 as follows

$$\lambda = \frac{3}{4\pi} \frac{M_5^6}{M_4^2}. \quad (4)$$

$M_p = M_4/\sqrt{8\pi}$ is the reduced Planck mass. The nucleosynthesis limit implies $\lambda \gtrsim (1 \text{ MeV})^4 \sim (10^{-21})^4$ in reduced Planck units. A more stringent constraint can be obtained by requiring the theory to reduce to Newtonian gravity on scales larger than 1 mm corresponding to $\lambda \gtrsim 5 \times 10^{-53}$, i.e. $M_5 \gtrsim 10^5 \text{ TeV}$. Notice that in the limit $\lambda \rightarrow \infty$ we recover standard Friedman equation in four dimensions. Accordingly, we will work in the high energy regime where brane effects are appreciable with $V/\lambda \gg 1$.

The slow-roll parameters in brane scenario are modified into [23]

$$\epsilon = \frac{1}{2} \left(\frac{V'}{V} \right)^2 \frac{1}{\left(1 + \frac{V}{2\lambda} \right)^2} \left(1 + \frac{V}{\lambda} \right), \quad (5)$$

$$\eta = \left(\frac{V''}{V} \right) \left(\frac{1}{1 + \frac{V}{2\lambda}} \right). \quad (6)$$

And the number of e -foldings are calculated as

$$N = - \int_{\phi_*}^{\phi_e} \frac{V}{V'} \left(1 + \frac{V}{2\lambda} \right) d\phi. \quad (7)$$

In the low energy regime, $V/\lambda \ll 1$ or $\lambda \rightarrow \infty$, the usual definitions in standard cosmology are recovered. However, in the high energy regime, $V/\lambda \gg 1$, the slow-roll parameters ϵ and η are suppressed by a factor V/λ , so even steep potential easily satisfies the slow-roll conditions.

For the Randall-Sundrum model II [26], the amplitudes for the scalar and tensor power spectrum are [23, 27]

$$A_t = \frac{1}{150\pi^2} V \left(1 + \frac{V}{2\lambda}\right) F^2, \quad (8)$$

$$A_s = \frac{1}{75\pi^2} \frac{V^3}{V'^2} \left(1 + \frac{V}{2\lambda}\right)^3, \quad (9)$$

where

$$F^2 = \left[\sqrt{1+x^2} - x^2 \sinh^{-1} \left(\frac{1}{x} \right) \right]^{-1}, \quad (10)$$

and

$$x \equiv \left(\frac{3H^2}{4\pi\lambda} \right)^{1/2} = \left[\frac{2V}{\lambda} \left(1 + \frac{V}{2\lambda}\right) \right]^{1/2}. \quad (11)$$

The spectral tilt for scalar perturbation can be written in terms of the slow-roll parameters as [23]

$$n_s = 1 - 6\epsilon + 2\eta, \quad (12)$$

and the tensor-to-scalar ratio is [28]

$$r = 16 \frac{A_t}{A_s}. \quad (13)$$

In the low-energy limit, $V/\lambda \ll 1$, $F^2 \approx 1$, we recover the standard result $r = 16\epsilon$. While in the high energy limit, $V/\lambda \gg 1$, $F^2 \approx 3V/2\lambda$, the tensor-to-scalar ratio is modified into $r = 24\epsilon$ and the amplitude for the tensor power spectrum becomes

$$A_t = \frac{V}{50\pi^2} \left(\frac{V}{2\lambda} \right)^2. \quad (14)$$

So the energy scale of inflation and the brane tension cannot be fixed by the observational values of A_s and r .

III. NUMERICAL RESULTS

We numerically calculate the inflationary predictions and check the consistency conditions for both $m = 1$ and $m = 2$ models. The selected inflation path is between the origin and the turning point $\phi_t = \beta^{-1}(m^{-1}n)^{\frac{1}{m}}$ as indicated in Figure 1.

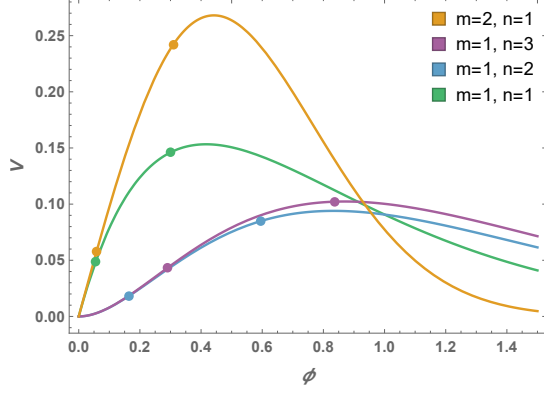


FIG. 1. Potentials for models with $m = 1, 2$. The parameters β and α are chosen to be consistent with the Planck observations $n_s = 0.965$ and $A_s = 2.10 \times 10^{-9}$. The points represent ϕ_* and ϕ_e .

Figure 2 gives the 1σ and 2σ results of scalar spectral index n_s and tensor-to-scalar ratio r for both types of models. We set the number of e -folds to be $N = 60$ and let the two parameters α/λ and β vary independently with the sub-planckian field excursions condition $\Delta\phi < 1$ imposed.

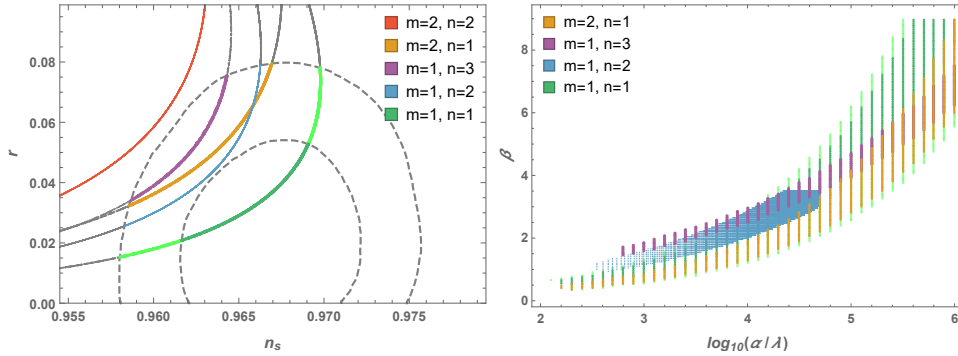


FIG. 2. $n_s - r$ plane for $m = 1, 2$ models with $N = 60$ and $\Delta\phi < 1$. The dashed contours come from Planck 2018 data [20]. In the right panel, 1σ and 2σ constrained parametric space for $\log_{10}(\alpha/\lambda)$ and β is shown with the corresponding colors.

It can be seen from Figure 2 that the model parameters α/λ and β are correlated. The value of β increases as α/λ increases. Hence, we just need to determine the lower limits for the parameters $(\alpha/\lambda; \beta)$. For the models $m = 1, n = 1$ and $m = 1, n = 2$, the lower limits are (150; 0.65) and (350; 1), for the models $m = 2, n = 1$ and $m = 1, n = 2$, they are (150; 0.45) and (900; 0.8) in reduced Planck units.

For all the models inflation ends at $\epsilon = 1$ since $|\eta|$ is always smaller than ϵ at the inflation

exit point. For models with $m = 1$, the slow-roll parameter η is

$$\begin{aligned}\eta &= \left(\frac{V''}{V}\right) \left(\frac{1}{1 + \frac{V}{2\lambda}}\right) \\ &= \left(\frac{n}{\phi} \left(\frac{n-1}{\phi} - 2\beta\right) + \beta^2\right) \left(\frac{1}{1 + \frac{V}{2\lambda}}\right).\end{aligned}\quad (15)$$

For models under the consideration, $\lambda/\alpha \ll 1$, we can expand the number of e -foldings N , the spectral index n_s , and the tensor-to-scalar ratio r up to first order in λ/α as

$$N \approx \frac{\alpha}{2\beta^3\lambda} \left(e^{-\beta\phi}(\beta\phi + 2) + \frac{\text{Ei}(1 - \beta\phi)}{e} \right) \Big|_{\phi_e}^{\phi_*} + \mathcal{O}(\lambda/\alpha)^2, \quad (16)$$

$$n_s(\phi_*) \approx 1 - \frac{4\beta^3\lambda e^{\beta\phi_*} (2\beta^2\phi_*^2 - 4\beta\phi_* + 3)}{\alpha (\beta\phi_*)^3} + \mathcal{O}(\lambda/\alpha)^2, \quad (17)$$

$$r(\phi_*) \approx \frac{48\beta^3\lambda e^{\beta\phi_*} (1 - \beta\phi_*)^2}{\alpha (\beta\phi_*)^3} + \mathcal{O}(\lambda/\alpha)^2, \quad (18)$$

where $\text{Ei}(x)$ is the exponential integral. It is apparent from Eq. (16) that $\beta\phi_*$ is a function of $(\beta^3\lambda N)/\alpha$. Similarly from Eqs. (17) and (18) both n_s and r depend on $(\beta^3\lambda)/\alpha$ for a fixed N . This explains our numerical results in Figure 2 where we obtained a single curve for each model with two varying parameters α/λ and β , which, effectively combine into a single one $\alpha/(\beta^3\lambda)$. Furthermore, for $N = 60$, we should have $\alpha/(\beta^3\lambda) \gtrsim 10^2$ to ensure that the spectral index remains less than unity. Hence the parameters α/λ and β are bounded from below as can be seen from the right panel in Figure 2.

In order to realize the observed power spectrum $A_s = 2.10 \times 10^{-9}$, either λ or α should be adjusted accordingly. In Figure 3, the range of $A = \alpha/\lambda$ in $m = 1$, $n = 1$ model with $\beta = 2$ is given. Comparing with the 2018 Planck results [20], when $A \in [4000, 15000] \text{ M}_p^{-2}$, the spectral index of scalar perturbations n_s locates in the 68% CL bound of $n_s = 0.9649 \pm 0.0042$. In this parametric region, the tensor-to-scalar ratio r is significantly smaller than its upper bound $r_{0.05} < 0.06$. To realize $A_s = 2.10 \times 10^{-9}$, we need $\alpha \in [1.5 \times 10^{-14}, 5.5 \times 10^{-14}] \text{ M}_p^3$ and $\lambda \in [1.1 \times 10^{-18}, 1.4 \times 10^{-17}] \text{ M}_p^5$. Hence for $\beta \sim 2$ and $\alpha/\lambda \sim 10^4 \text{ M}_p^{-2}$, the typical values are $\alpha \sim 10^{-14} \text{ M}_p^3$ and $\lambda \sim 10^{-18} \text{ M}_p^5$.

Figure 1 shows the potentials for models with $m = 1, 2$. The inflation ends when the slow-roll condition $\epsilon = 1$ is satisfied. The points in Figure 1 correspond to ϕ_* and ϕ_e . Here, the parameters α and β are chosen to be consistent with the Planck observations. As we can see, β is $\mathcal{O}(1)$ to ensure 60 e -foldings. The parameters and results are also given in Table I.

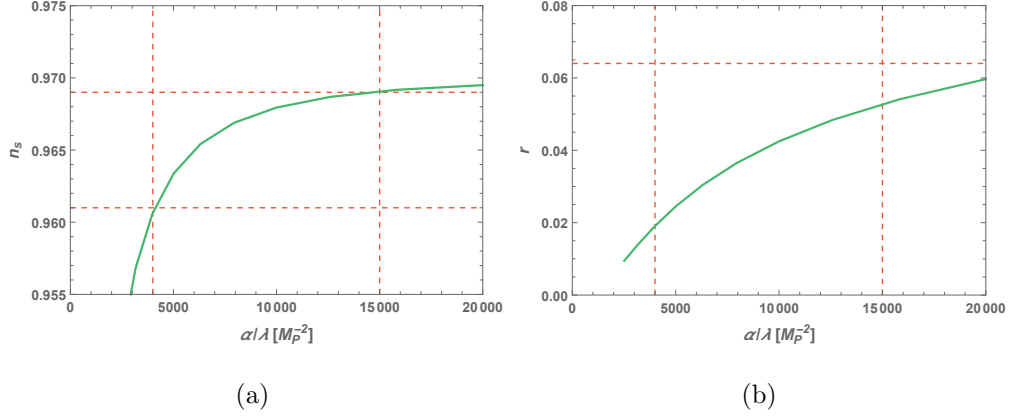


FIG. 3. Result for $m = 1$, $n = 1$ model, $A = \alpha/\lambda$ is the variable with $\beta = 2$ and $N = 60$. The vertical lines locate at $A_1 = 4000 \text{ M}_\text{p}^{-2}$ and $A_2 = 15000 \text{ M}_\text{p}^{-2}$. The horizontal lines in (a) correspond to the 68% CL bound of $n_s = 0.9649 \pm 0.0042$ [20]. 95% CL upper bound on the tensor-to-scalar ratio from Planck 2018 combined with the BICEP2/Keck Array BK14 data is $r_{0.05} < 0.06$ [20] which is given as the horizontal line in (b).

(m,n)	β	$\alpha(10^{-14}\text{M}_\text{p}^3)$	n_s	r	$\phi_*(\text{M}_\text{p})$	$\phi_e(\text{M}_\text{p})$
(1,1)	2.39	2.38	0.9649	0.0289	0.3003	0.0555
(1,2)	2.37	21.63	0.9649	0.0541	0.5954	0.1657
(1,3)	2.33	39.98	0.9646	0.0900	0.8373	0.2906
(2,1)	1.56	1.04	0.9650	0.0591	0.3087	0.0579

TABLE I. α/λ is 10^4 , and e -foldings $N = 60$.

In Figure 4 we plot the n_s and r against the field excursion $\Delta\phi$ with $N = 60$ e -folds for various $m = 1, 2$ models considered here. It can be seen clearly that the field excursion remains sub-planckian as to avoid the quantum gravity corrections that may break the effective field description due to quantum gravity corrections as advocated in distance conjecture [29].

IV. CONCLUSIONS

We analyzed a class of potentials in braneworld inflation numerically and analytically. The class of potentials $V(\phi) = \alpha\phi^n \exp(-\beta^m \phi^m)$ were obtained in supergravity with a small shift symmetry breaking term in the Kähler potential.

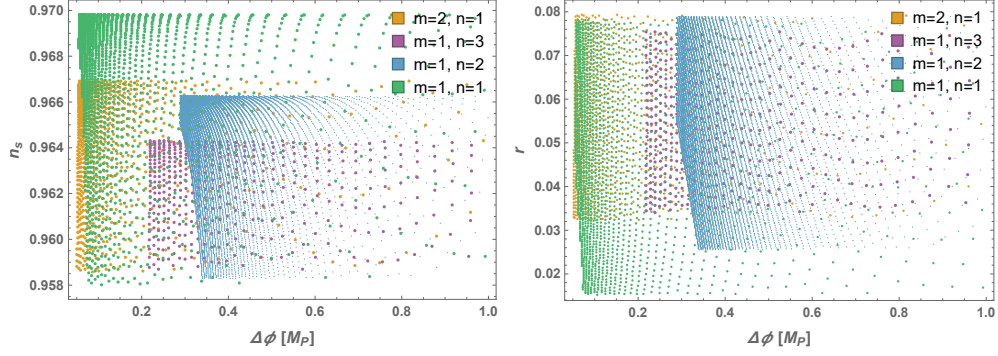


FIG. 4. Left panel shows the plot of n_s and field excursion $\Delta\phi$ while the right panel shows the plot of r versus $\Delta\phi$ for $m = 1, 2$ models with $N = 60$ e -foldings.

In the high energy regime $\alpha/\lambda \gg 1$ where the brane correction is important, the observables n_s and r depend on a single parameter $\beta^3\lambda/\alpha$ although there are three independent parameters λ , β and α in the model. This novel and interesting result is apparent from numerical analysis and shown explicitly with analytical approximation for the model with $m = n = 1$. The sub-Planckian field inflation models with $m = 1$ and $m = 2$ accommodate the Planck 2018 observational constraints. The inflation models with smaller n are preferred while the models with larger n are out of the 2σ bound in $n_s - r$ plane. In particular, the model with $m = 1$ and $n = 1$ is consistent with the Planck observations at the 1σ confidence level.

In braneworld the slow-roll conditions can even be satisfied for otherwise steep potentials and the amount of inflation between any two points in the potential is greater than the one obtained in standard cosmology. The corresponding field excursions also stay sub-Planckian. The primordial gravitational waves associated to the obtained value of $r \sim 10^{-2}$ might be detected with the future LiteBIRD satellite.

ACKNOWLEDGMENTS

MS was supported by Higher Education Commission Pakistan Ph.D. scholarship. This research was supported by the Projects 11475238, 1605049, 11647601, 11875062, and 1187513 supported by the National Natural Science Foundation of China, by the Major Program of the National Natural Science Foundation of China under Grant No. 11690021, by the Key Research Program of Frontier Science (CAS), and by the Scientific Research Program

- [1] A. A. Starobinsky, *Phys. Lett. B* **91**, 99 (1980), [Adv. Ser. Astrophys. Cosmol.3,130(1987)].
- [2] A. H. Guth, *Phys. Rev. D* **23**, 347 (1981), [Adv. Ser. Astrophys. Cosmol.3,139(1987)].
- [3] A. D. Linde, *QUANTUM COSMOLOGY*, *Phys. Lett. B* **108**, 389 (1982), [Adv. Ser. Astrophys. Cosmol.3,149(1987)].
- [4] A. Albrecht and P. J. Steinhardt, *Phys. Rev. Lett.* **48**, 1220 (1982), [Adv. Ser. Astrophys. Cosmol.3,158(1987)].
- [5] L. Wu, S. Hu, and T. Li, *Eur. Phys. J. C* **77**, 168 (2017), [arXiv:1605.00735 \[hep-ph\]](#).
- [6] Z. Yi, Y. Gong, and M. Sabir, *Phys. Rev. D* **98**, 083521 (2018), [arXiv:1804.09116 \[gr-qc\]](#).
- [7] W. Ahmed and A. Karozas, *Phys. Rev. D* **98**, 023538 (2018), [arXiv:1804.04822 \[hep-ph\]](#).
- [8] M. Sabir, W. Ahmed, Y. Gong, T. Li, and J. Lin, (2019), [arXiv:1908.05201 \[hep-ph\]](#).
- [9] M. Sabir, W. Ahmed, Y. Gong, and Y. Lu, *Eur. Phys. J. C* **80**, 15 (2020), [arXiv:1903.08435 \[gr-qc\]](#).
- [10] C. Cheung, P. Creminelli, A. L. Fitzpatrick, J. Kaplan, and L. Senatore, *JHEP* **03**, 014 (2008), [arXiv:0709.0293 \[hep-th\]](#).
- [11] D. H. Lyth, *Phys. Rev. Lett.* **78**, 1861 (1997), [arXiv:hep-ph/9606387 \[hep-ph\]](#).
- [12] Q. Gao, Y. Gong, and T. Li, *Phys. Rev. D* **91**, 063509 (2015), [arXiv:1405.6451 \[gr-qc\]](#).
- [13] A. Suzuki *et al.*, *17th International Workshop on Low Temperature Detectors (LTD 17) Kurume, Japan, July 17-21, 2017*, *J. Low. Temp. Phys.* **193**, 1048 (2018), [arXiv:1801.06987 \[astro-ph.IM\]](#).
- [14] J. M. Maldacena, *Int. J. Theor. Phys.* **38**, 1113 (1999), [Adv. Theor. Math. Phys.2,231(1998)], [arXiv:hep-th/9711200 \[hep-th\]](#).
- [15] E. Witten, *Adv. Theor. Math. Phys.* **2**, 253 (1998), [arXiv:hep-th/9802150 \[hep-th\]](#).
- [16] D. Harlow and H. Ooguri, (2018), [arXiv:1810.05338 \[hep-th\]](#).
- [17] D. Z. Freedman, P. van Nieuwenhuizen, and S. Ferrara, *Phys. Rev. D* **13**, 3214 (1976).
- [18] S. Deser and B. Zumino, *Phys. Lett. B* **62**, 335 (1976).
- [19] T. Li, Z. Li, and D. V. Nanopoulos, *JCAP* **1402**, 028 (2014), [arXiv:1311.6770 \[hep-ph\]](#).
- [20] Y. Akrami *et al.* (Planck), (2018), [arXiv:1807.06211 \[astro-ph.CO\]](#).
- [21] T. Shiromizu, K.-i. Maeda, and M. Sasaki, *Phys. Rev. D* **62**, 024012 (2000), [arXiv:gr-](#)

- qc/9910076 [gr-qc].
- [22] C. Csaki, M. Graesser, C. F. Kolda, and J. Terning, *Phys. Lett. B* **462**, 34 (1999), [arXiv:hep-ph/9906513 \[hep-ph\]](#).
 - [23] R. Maartens, D. Wands, B. A. Bassett, and I. Heard, *Phys. Rev. D* **62**, 041301 (2000), [arXiv:hep-ph/9912464 \[hep-ph\]](#).
 - [24] P. Binetruy, C. Deffayet, U. Ellwanger, and D. Langlois, *Phys. Lett. B* **477**, 285 (2000), [arXiv:hep-th/9910219 \[hep-th\]](#).
 - [25] P. Binetruy, C. Deffayet, and D. Langlois, *Nucl. Phys. B* **565**, 269 (2000), [arXiv:hep-th/9905012 \[hep-th\]](#).
 - [26] L. Randall and R. Sundrum, *Phys. Rev. Lett.* **83**, 4690 (1999), [arXiv:hep-th/9906064 \[hep-th\]](#).
 - [27] D. Langlois, R. Maartens, and D. Wands, *Phys. Lett. B* **489**, 259 (2000), [arXiv:hep-th/0006007 \[hep-th\]](#).
 - [28] M. C. Bento, R. G. Felipe, and N. M. C. Santos, *Phys. Rev. D* **77**, 123512 (2008), [arXiv:0801.3450 \[astro-ph\]](#).
 - [29] G. Obied, H. Ooguri, L. Spodyneiko, and C. Vafa, (2018), [arXiv:1806.08362 \[hep-th\]](#).